IEEE Access
Multidisciplinary | Rapid Review | Open Access Journal

Received February 22, 2019, accepted April 1, 2019, date of publication April 3, 2019, date of current version April 25, 2019.

Digital Object Identifier 10.1109/ACCESS.2019.2909153

Reliability Modeling and Assessment of Isolated Microgrid Considering Influences of Frequency Control

JING GUO[1], TIANYANG ZHAO[2], (Member, IEEE), WENXIA LIU[1], AND JIANHUA ZHANG[1], (Member, IEEE)

[1]State Key Laboratory of Alternate Electrical Power System with Renewable Energy Sources, North China Electric Power University, Beijing 102206, China
[2]Energy Research Institute, Nanyang Technological University, Singapore 639798

Corresponding author: Tianyang Zhao (matrixeigs@gmail.com)

This work was supported in part by the National Key R&D Program of China under Grant 2017YFB0903100, and in part by the Science and Technology Foundation of SGCC under Grant 521104170043.

ABSTRACT Frequency control of isolated microgrid (MG) relies heavily on a safe and reliable cyber system. Random failures of cyber elements may cause the malfunction of the frequency control, resulting in reliability issues, e.g., load shedding or generation curtailment. A reliability modeling and assessment method for isolated MG is proposed, considering the influence of frequency control from cyber physical system perspectives. The frequency control process is modeled to establish the interdependencies between a cyber system and physical system within MGs. An assessment method is proposed to quantify the impacts of cyber element failures based on the frequency control models. A set of novel reliability index is defined to illustrate impacts of frequency control malfunction on the MG reliability. The sequential Monte Carlo simulation method is adopted to assess the reliability of MGs considering the malfunction of frequency control. The effectiveness of proposed models and indices is demonstrated by the case studies on an isolated MG. The test results indicate that the frequency control malfunction caused by the failures of cyber elements has a great impact on MG reliability. This research can provide technical support for the planning and operation of isolated MGs.

INDEX TERMS Cyber physical system, frequency control, isolated microgrid, reliability assessment, sequential Monte Carlo.

I. INTRODUCTION

The MICROGRIDS (MGs) are cyber physical systems (CPSs) [1], where the physical system is a small power system that integrates distributed energy resources, power distribution equipment and loads [2]. The cyber system is to monitor, control and manage the physical system, realizing the reliable, secure and efficient operation of MGs [3]. The control system within MGs is always formulated as a hierarchal system, including primary, secondary and tertiary control [4]. The failures of cyber systems or malfunctions of control systems may result in load shedding or generation curtailment that will affect the reliability of MGs [5], [6]. Modelling MGs from CPS approaches, to reveal the interdependence relationships between cyber and physical systems, is of importance for ensuring the reliable operation of MGs.

Reliability assessment of power CPSs, e.g., MGs and distribution systems, is one hot research topic recently, including cyber system reliability modeling [7]–[10], interdependence relationships modelling between cyber systems and physical systems [3], [7]–[14], and *etc*. In the reliability models for cyber systems, the two-state models [7], [8] have been extended to the information dynamic transmission performance models [9], [10], accounting for impacts of communication failures, e.g., transmission error and delays.

The interdependence relationships between the cyber system and physical system have been addressed from the direct [7] and indirect [12] interdependency perspectives. The direct interdependency (DI) indicates that any failure

The associate editor coordinating the review of this manuscript and approving it for publication was Davide Aloini.

of cyber element results in the failure of a corresponding element in the physical network [7], [9], [11]. For instance, the failure of feeder protection element or the breaker controller are equivalent to the breaker disconnected [9]. The indirect interdependency (II) means that failure of cyber element does not directly cause the failure or change of the element behaviors in the physical system, but will affect the system performance. For example, the impacts of monitoring and protection elements on substation reliability and the transmission delays and errors on distribution network and MG are assessed in [12], [9] and [10], respectively. Existing literatures show that the potential failure of II has greater impacts to the system reliability [9]–[14].

Considering different interdependence relationships, e.g., DI and II, the impacts of cyber element failures on the physical system should be assessed in specific physical process with corresponding models. For the DI, the serial model is usually adopted to characterize this relationship, e.g., superimposing the cyber element failure rate into the physical element [7], [9]. For the II, due to the hidden relationship between element failures and system states, it is necessary to model the cyber system and physical system jointly for the impacts assessment of cyber element failures. In [9], the impacts of monitoring and fault handling elements failures on the load shedding are quantified in the distribution network restoration, including the extension of power outage duration and *etc*. In [10], the impacts of cyber element failures and the transmission interference on MG reliability are analyzed based on the method of simulating the operation of the MG.

For the reliability assessment of power CPSs with II failures, a systemic model for cyber system and physical system should proposed in accordance with the physical systems, where the control system should be embedded into the cyber systems. Compared with the distribution networks, the isolated MGs (IMGs) are low inertia and more vulnerable in face of cyber element failure [15]. The failures of cyber elements not only lead to the load shedding but also result in the malfunction of control systems under II failures, affecting the frequency and voltage control functions, resulting in load shedding or blackout. According to the best of knowledge, the hidden relationship between the cyber element failures and IMG's reliability has not been addressed with control system models.

In this paper, a reliability modeling and assessment method for IMGs from cyber physical system perspectives is proposed, considering the malfunction of frequency control. The main contributions of this paper can be summarized as follows: (1) the cyber physical DI and II are established considering the malfunction of frequency control; (2) a quantitative assessment method for malfunction of frequency control is proposed; (3) a set of novel reliability indices are proposed to illustrate hidden impacts of the cyber element failures on IMG reliability, accordingly.

The rest of this paper is organized as follows. In Section II, the topology of IMG is introduced and the cyber physical DI and II are established. In Section III, the element reliability models are proposed including element reliability model and power state generation in reliability assessment. The quantitative assessment methods for cyber element failure consequences are presented In Section IV. In Section V, a set of novel reliability index is established and IMG reliability assessment process considering frequency control is proposed. A case study is performed in Section VI to illustrate the performance of the proposed models and assessment methods. In Section VII, conclusion and remarks are drawn.

II. IMG CYBER-PHYSICAL SYSTEM

To depict the interdependency between the element failures and system reliability in frequency control, IMGs are modelled from the cyber physical system perspectives in this section, including the IMG cyber-physical system, frequency control and interdependency analysis.

A. IMG CYBER PHYSICAL SYSTEM

IMGs, as cyber physical systems, include both physical system and cyber system. The physical system of IMG includes circuit breakers, transmission lines, transformers and distributed energy resources (DERs), e.g., wind turbine generators (WTGs), photovoltaics (PVs), energy storage systems (ESSs) and diesel generators (DGs). Its function is to generate, transmit and distribute of electrical energy within local areas. The cyber system includes information collection equipment, various types of controllers and communication equipment, e.g., the MG control center (MGCC), the public coupling connector (PCC), the micro-source controller (MC) and load controller (LoC), circuit breaker controller (CBC), potential transformer (PT), current transformer (CT), network switch (SW) and optical fiber lines. It is responsible for state sensing and device control of the physical systems.

Two types of control schemes are widely adopted for IMGs, i.e., centralized and distributed. In the centralized control, the stable operation is ensured by the MGCC via collecting system data and issuing control commands. In the distributed control, the MGCC is replaced by decision makers distributed throughout the networks. The calculation and issuance of control command are completed by specific decision maker, according to its own and neighboring decision makers' information. Considering the sources are located closely, the centralized control scheme is widely adopted in practice [16], [17]. In this paper, the reliability of IMGs is assessed under the centralized control scheme, as shown in Fig. 1, where the connection relationship between cyber and power systems is illustrated [18], [19].

B. FREQUENCY CONTROL OF IMG

A hierarchical three level control structure is employed for the frequency control of IMGs, which is performed in the centralized way [4], [20]. The primary control is responsible for properly control the DER units through the MCs as well as pursuing the power balance locally [21]. In the secondary control, the system frequency deviation is monitored by the

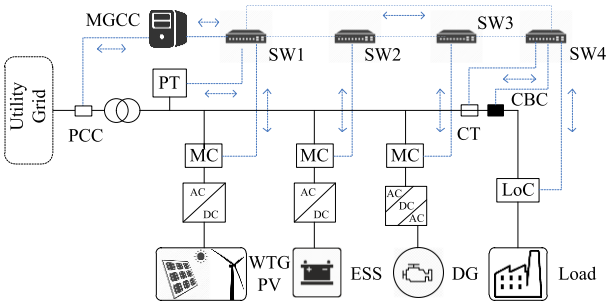

FIGURE 1. Schematic diagram of IMG.

MGCC and the adjustment values are calculated and assigned to the respective DER units to maintain the frequency at the rated value [22], [23]. Based on renewable energy and load forecasting information, the controllable DER output is optimized in the tertiary control level via economic dispatch and *etc*. The hierarchical control scheme is shown in Fig. 2.

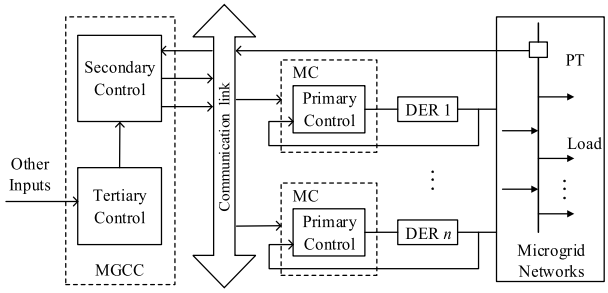

FIGURE 2. Frequency control scheme of IMG.

As shown in the Fig. 2, the information flow in the frequency control process can be analyzed.

1) Primary control: The three-phase voltage and current signals are acquired locally at MCs, and the primary frequency control value is calculated by the power calculation module and droop control module in MCs and transmitted to the DERs.

2) Secondary control: The three-phase voltage signals are acquired by the PT installed on the bus and transmitted to the MGCC through the SWs and the communication lines. The secondary frequency adjustment value is calculated by the MGCC and assigned to the MC through the SWs and communication lines [23].

3) Tertiary control: The set points of DERs are calculated by the MGCC based on the power and load forecasting and are sent to the MCs through the SWs and communication lines.

C. CYBER PHYSICAL INTERDEPENDENCIES IN FREQUENCY CONTROL

Cyber elements can be divided into two categories based on cyber physical schematic diagram and frequency control scheme. One is the DI cyber element. For instance, if the MCs fail, the MGCC and the system stability controller cannot monitor and control the related DERs. To ensure the secure and stable operation of MGs, DERs should be turned off under this circumstance [7]. When the CBC and CT fail, the system stability controller cannot detect and control the circuit breaker devices, indicating this circuit breaker is operating under an unprotected state. This circuit should be disconnected by the stability controller to prevent potential damages to the electrical equipment [9].

The other is the II cyber element, that is, the failure of cyber elements does not directly cause the physical elements to fail, but results in the malfunction of frequency control. As described above, the failure of the II cyber element might result in 1) the input information is blocked, 2) loss or delay of measurement/control signals, 3) abnormal control signal from MGCC due to the input information error. For example, if the information acquisition device (PT) and the computing device (MGCC) associated to the secondary frequency control fail, or the network SWs connected to the MGCC, PT and controllable DERs fail, the controllable DERs cannot receive the secondary frequency control signals. However, since the controllable DERs still have the ability to perform primary control, the frequency control mode is switched from the centralized control mode to the local control mode, and the frequency is adjusted by the droop control locally. The DI and II cyber elements to the physical system are summarized in Table 1.

TABLE 1. Cyber physical interdependencies.

Faulty elements	Inter-dependencies	Related elements/systems	Failure consequences
MC	DI	DERs	DERs are turned off.
CBC/CT		Circuit breakers	Circuit breakers are disconnected.
MGCC PT SW	II	Frequency control system	Switched from the centralized frequency control mode to the local control mode.

III. IMG RELIABILITY MODELING

For the reliability assessment on IMGs, the following three steps are performed: 1) system status generation, 2) failure consequence analysis and 3) reliability indices calculating. In the first step, fault status sampling and DERs' output states at the failure moment are generated. The former is obtained by sampling the elements using the two state models shown in section III.A, including start and end time of the faulty element, and the latter is obtained by solving the IMG tertiary frequency control models in section III.B. The second step and the third step are depicted in section IV and section V, respectively.

A. TWO STATE MODELS OF CYBER PHYSICAL ELEMENTS

For the reliability assessment, the two state models are widely adopted for the cyber elements [9], [10], [24], i.e., normal

state and fault state. In the process of the sequential Monte Carlo (SMC) simulation method, a sequential state transition process of the system can be formed using the sampling of element status. Assuming that the element failure rate λ (time / year) and repair rate μ (time / year) are constant, and the working time and repair time are subject to the exponential distribution, the failure probability P_{failure} and repair probability P_{repair} before time t are expressed as follows

$$P_{\text{failure}} = 1 - e^{-\lambda t} \tag{1}$$
$$P_{\text{repair}} = 1 - e^{-\mu t} \tag{2}$$

The mean time between failures t_{mtbf} and mean time to repair t_{mttr} can be expressed as follows

$$t_{mtbf} = \int_0^{\infty} t \cdot \lambda e^{-\lambda t} dt = -(1/\lambda) \cdot \ln(x_1) \tag{3}$$
$$t_{mttr} = \int_0^{\infty} t \cdot \lambda e^{-\mu t} dt = -(1/\lambda) \cdot \ln(x_2) \tag{4}$$

where x_1 and x_2 are random variables, following uniform distributions in [0,1]. In addition, the physical elements in IMGs can be modelled using the same approach, i.e., Eq.(1) - Eq.(4). The probabilistic output models of WTGs and PVs are referred to [25] and are not described here.

B. TERTIARY FREQUENCY CONTROL MODEL OF IMG

Controllable DERs' outputs during the element failure periods can be obtained by solving multi-period optimization models of tertiary frequency control. Take the IMG, which includes two controllable DERs, DG and battery energy storage system (BESS), as an example. The tertiary frequency control is performed to minimize the operating cost, where the objective function can be expressed as follows

$$\min f = \sum_{t=1}^{T} \left[\sum_{i \in G} \left(c_{DG,i}(t) + m_{DG,i}(t) \right) + \sum_{i \in B} \left(m_{BESS,i}(t) \right) \right] \tag{5}$$

where G and B are sets of the DG and BESS, respectively. $c_{DG,i}(t)$ and $m_{DG,i}(t)$ are fuel cost function and maintenance cost function of the DG, respectively. $m_{BESS,i}(t)$ is the BESS cost function considering the depth of charge and discharge. T represents the simulation period. The detailed expressions of cost in Eq. (5) are depicted as follows

$$c_{DG,i}(t) = A\left(d + eP_{DG,i}(t) + fP_{DG,i}^2(t)\right) \tag{6}$$
$$m_{DG,i}(t) = k_{DG} \cdot P_{DG,i}(t) \tag{7}$$
$$m_{BESS,i}(t) = \frac{C_{init}}{N_{SB}(x)} \cdot \frac{k_{ch}}{P_{BESS}^c(t) \cdot S_{ocstart}} \cdot \frac{S_{ocend}}{S_{oc\max}} + \frac{C_{init}}{N_{SB}(x)} \cdot \frac{k_{dch}}{P_{BESS}^d(t) \cdot S_{ocend}} \cdot \frac{S_{ocstart}}{S_{oc\max}} \tag{8}$$
$$N_{SB}(x) = -3278x^4 - 5x^3 + 12823x^2 - 14122x + 5112 \tag{9}$$

where $P_{DG,i}(t)$ is the active output of diesel generator i at time t. A, d, e and f are the fuel cost coefficients. k_{DG} is the maintenance cost factor. C_{init} is the investment cost of BESS. $S_{oc\max}$ and $S_{oc.min}$ is the upper and lower limit of the SOC. $N_{SB}(x)$ is the maximum number of cycles of BESS. $x(x \in [0,1])$ is the BESS charge and discharge depth. BESS operating cost $m_{BESS,i}(t)$ is affected by the start and end state of charge $S_{ocstart}$, S_{ocend}, charge and discharge power $Pc\ BESS(t)$, $Pd\ BESS(t)$, and charge and discharge influence factors k_{ch}, k_{dch}. The active power balance constraints, BESS operating constraints, DER active output upper and lower bound constraints are shown as follows

$$\sum_{i \in G} P_{DG,i}(t) + \sum_{i \in B} P_{BESS,i}(t) + \sum_{i \in RG} P_{RG,i}(t) = \sum_{i \in L} P_{L,i}(t) \tag{10}$$
$$P_{DG,i}^{\min} \le P_{DG,i}(t) \le P_{DG,i}^{\max} \tag{11}$$
$$\left| P_{DG,i}(t) - P_{DG,i}(t-1) \right| \le R_i^{up} \tag{12}$$
$$S_{oc\min} \le S_{oc}(t) \le S_{oc\max} \tag{13}$$
$$p_{BESS}^c(t) p_{BESS}^d(t) = 0 \tag{14}$$
$$0 \le p_{BESS}^c(t), p_{BESS}^d(t) \le p_{BESS,\max} \tag{15}$$
$$S_{oc}(t) = S_{oc}(t-1) + [\eta_c \Delta T p_{BESS}^c(t) - (1/\eta_d)\Delta T p_{BESS}^d(t)]/S_{nom} \tag{16}$$

where RG is the set of renewable energy. $P_{L,i}(t)$ is the active load at time t. $Pmin\ DG,i$and $Pmax\ DG,i$ are the upper and lower output limits of DG. $Rup\ i$ is the maximal limitation that the DG's active output can increase or decrease in the [t-1, t] time slot. $P_{BESS,max}$ is the maximal charge and discharge rate limitation of BESS. $S_{oc}(t)$ and $S_{oc}(t\text{-}1)$ are the SOC at time slot t and time t-1, respectively. η_c and η_d are BESS charge and discharge efficiencies. S_{nom} is the rated capacity of BESS.

IV. ELEMENT FAILURE CONSEQUENCE ANALYSIS

Elements that affect the reliability of IMGs can be classified into the following three types: 1) physical elements, 2) DI cyber elements, and 3) II cyber elements. The consequence of each type of element failure is analyzed in this section, using its corresponding model.

A. PHYSICAL ELEMENT FAILURE CONSEQUENCE ANALYSIS

The system is traversal searched by traversing search algorithm [10]. Depending the connection relationship between the loads and IMGs, the loads can be classified into the following two types, i.e., loads connected with the IMGs and loads disconnected from the IMGs. The loads, disconnected from the IMGs, will be blacked out until the faulty element is repaired. The loads, connected to the IMGs, are assessed

by calculating the balance between DERs output and the load information. If not all loads are satisfied, some loads will be shed. For load point i, the number of power outages $C_{P,i}$, the load blackout duration $U_{P,i}$ and the loss of load $E_{P,i}$ during the restoration of a single element can be calculated as follows

$$C_{P,i} = \begin{cases} 0 \ if \ \sum P_{OMS}(t_P) \geq \sum P_{load}(t_P) \\ 1 \ if \ \sum P_{OMS}(t_P) < \sum P_{load}(t_P) \end{cases} \quad (17)$$

$$U_{P,i} = C_{P,i}(t_P) \cdot (t_{pn} - t_p) \quad (18)$$

$$E_{P,i} = \sum_{t_p}^{t_{pn}} P_{lshed,i}(t_p) \quad (19)$$

where t_{pn} is the end time of the element fault duration and is sampled using Eq. (4). $t_p = 1, 2, \cdots, t_{pn}$. $\sum P_{OMS}(t_p)$ is the sum of the output of DERs except the faulty DER at the time of t_p and $\sum P_{load}(t_p)$ is the total load demand. $P_{lshed}(t_p)$ is the amount of load shed in the t_p.

B. DI CYBER ELEMENT FAILURE CONSEQUENCE ANALYSIS

The cyber physical relationship is described in the adjacency matrix which is established by the method in reference [10] and the DI cyber element's failure will be equivalent to the corresponding physical element. Then the load blackout indices can be calculated using Eq. (17) ∼ (19).

C. II CYBER ELEMENT FAILURE CONSEQUENCE ANALYSIS

Secondary frequency control might fail when cyber element fails under II. Without the coordination of secondary control, the system frequency may not be maintained within the predefined range, due to the limitation of primary control [4]. When the frequency exceeds the upper and lower limits, the loads or generators will be shut down by the MGCC to maintain the frequency within the range, which degrades system reliability. The frequency deviation under primary frequency control should be solved first.

Each controllable DER in the IMGs is assumed to adopt the *P-f* droop control to participate in the primary frequency regulation, and the frequency deviation can be compensated by the active output adjustment of these DERs. The controllable DER *P-f* droop control characteristic [16] is described as follows

$$f = f_{ref} - m_p(P_g - P_{ref}) \quad (20)$$

where f is the system frequency, P_g is the output power of the DER, f_{ref} and P_{ref} are the reference of frequency and active power, respectively. m_p is the frequency droop control coefficient. In the steady-state analysis, it is assumed that the system dynamics including the transient and oscillating modes are all damped out and power system is reached to a stable equilibrium point [17], as follows

$$\sum_{i=1}^{N_g} A_i^{DG} \cdot \Delta P_{g,i} = \sum_{l=1}^{N_l} \Delta L_l - \sum_{w=1}^{N_w} \Delta P_{wt,w} - \sum_{v=1}^{N_v} \Delta P_{pv,v} + D_{load} \cdot \Delta f - L_s \quad (21)$$

where N_g, N_l, N_w and N_v represent the number of controllable DERs, load points, WTGs, and PVs, respectively. *ADG i* is the operating state of the i-th controllable DER (0 or 1). $\Delta P_{g,i}$ is the active output adjustment amount of the i-th controllable DER. ΔL_l is the load variation of the l-th load point. $\Delta P_{wt,w}$ and $\Delta P_{pv,v}$ are the output variation of WTGs and PVs, respectively. Δf is the frequency variation. L_s is the amount of load forced to be shed. D_{load} is the steady state load frequency elastic coefficient of the IMG, defined as follows

$$D_{load} = L_{load}/f_{ref} \quad (22)$$

where L_{load} is the load level. The sum of the primary and the secondary frequency adjustment amount meets the system's active power deficiency, as shown in Eq. (20) and Eq.(21).

$$\sum_{i=1}^{N_g} \Delta P_{g,i} = \sum_{k=1}^{N_g^{sec}} P_{ref,k} - \sum_{i=1}^{N_g} \Delta f \cdot \left[1/m_p(i)\right] \quad (23)$$

where N_g^{sec} is the number of DERs participating in the secondary frequency control.$P_{ref,k}$ and Δf are the k-th DER active power output reference and system frequency deviation, respectively. $P_{ref,k}$ is calculated by the PI control module in MGCC. $m_p(i)$ is the droop coefficient of the i-th DER. According to Eq. (21) and Eq. (23), each DER's primary frequency control can be calculated as follows

$$\left(D_{load} + A_i^{DG} \cdot \left[1/m_p(i)\right]\right) \cdot \Delta f = -A_i^{DG} \cdot \Delta P_{g,i}^{pri} \quad (24)$$

where $\Delta P_{g,i}^{pri}$ is the primary frequency adjustment of the i-th DER. L_s, ΔL_l, PVs, and WTGs output are combined and calculated together. When the system only has the primary frequency control function, e.g., the MGCC is down, the system frequency can be stabilized at a certain value after the coordinated control of DERs. According to Eq. (24), the system steady-state frequency deviation Δf_{pri} can be calculated from the deviation of the active output, shown as follows

$$\Delta f_{pri} = -\frac{\sum_{i=1}^{N_g} A_i^{DG} \cdot \Delta P_g^{pri}}{D_{load} + \sum_{i=1}^{N_g} A_i^{DG} \cdot \left[1/m_p(i)\right]} \quad (25)$$

The system steady-state frequency $f_d (d = 1, 2, \cdots, t_{cn})$ can be calculated using Eq. (25). When $f_{min} \leq f_d \leq f_{max}$, the frequency is within the allowable range, where f_{min} and f_{max} are the lower and upper boundary of frequency. When $f_d < f_{min}$, some loads will be shed by MGCC according to the load shedding sequence, and the remaining loads continue to perform frequency control simulation until the

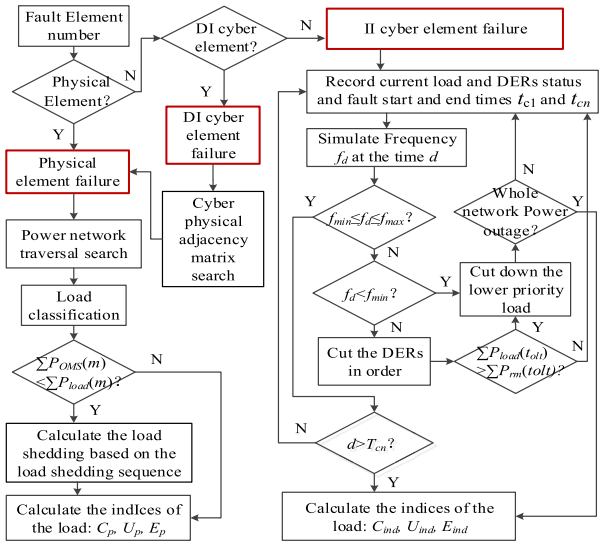

FIGURE 3. Failure consequences assessment process.

frequency requirement is met. The load shedding is calculated by balancing the balance of power and demand [10]. When $f_d > f_{max}$, some generators will be shut down by MGCC, where the renewable energy generators are shut down firstly and the controllable DERs are shut down secondly. During each frequency simulation process caused by element failures under II, each load and DER can only be cut once. The number of power outages C_{ind}, load blackout duration U_{ind} and the loss of load E_{ind} caused by the failures of cyber elements under II can be expressed as follows

$$C_{ind}(t_{olt}) = \begin{cases} 0 & if\ f_{\min} \le f_d \le f_{\max} \\ 1 & if\ f_d < f_{\min} \\ need\ to\ shut\ down\ some\ of\ DERs & if\ f_d > f_{\max} \end{cases} \quad (26)$$

$$U_{ind}(t_{olt}) = C_{ind}(t_{olt}) \cdot (t_{cn} - t_{olt}) \quad (27)$$

$$E_{ind}(t_{olt}) = C_{ind}(t_{olt}) \cdot \sum_{t_{olt}}^{t_{cn}} P_{lshed}(t_{olt}) \quad (28)$$

$$C_{ind} = \sum C_{ind}(t_{olt}) \quad (29)$$

$$U_{ind} = \sum U_{ind}(t_{olt}) \quad (30)$$

$$E_{ind} = \sum E_{ind}(t_{olt}) \quad (31)$$

where t_{cn} is the end time of the element failure. t_{olt} stands for the moment when the frequency crosses the limit. $C_{ind}(t_{olt})$, $U_{ind}(t_{olt})$ and $E_{ind}(t_{olt})$ are the times, the duration and the amount of load shed at t_{olt}. $\sum P_{load}(t_{olt})$ and $\sum P_{rm}(t_{olt})$ indicate the sum of the load demand and the sum of DERs output when the frequency crosses the upper limit. $P_{lshed}(t_{olt})$ is the load shed by the load shedding sequence at t_{olt}. In summary, the failure consequences assessment process of the three types of elements is illustrated in Fig. 3.

V. RELIABILITY ASSESSMENT OF IMG CONSIDERING FREQUENCY CONTROL

A. RELIABILITY INDEX CONSIDERING FREQUENCY CONTROL

Reliability of IMGs will be affected by the failure of the frequency control. Considering the failure of frequency control, traditional reliability indices have enhanced by a set of novel reliability indices. These indices are defined to assess the failures of both elements and control function. Factors affecting system reliability are shown in Fig. 4. In addition, the reliability index also includes the load point reliability index: average annual power outage frequency λ(time/year) and annual average power outage time U(hour/year).

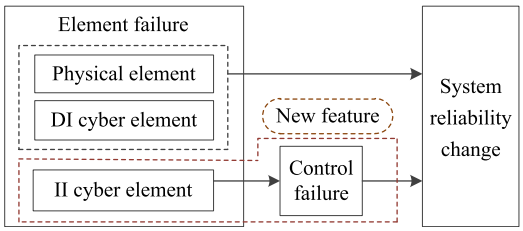

FIGURE 4. Factors affecting the system reliability.

1) Generalized system average interruption frequency index (*GSAIFI*): the average number of power outages per year due to element failure during the simulation period. The index is defined as follows

$$\text{GSAIFI} = \left[\sum_{i=1}^{n_l} n_{l,i}(C_{ef,i} + C_{ind,i})\right] / T \sum_{i=1}^{n_l} n_{l,i} \quad (32)$$

where n_l is the number of load points, and $n_{l,i}$ is the number of users of the i-th load point. T represents the simulation period. $C_{ind,i}$ and $C_{ef,i}$ represent the number of outage times at the load point i due to control malfunction or power interruption within the research period T, respectively. The calculation method of $C_{ind,i}$ is shown in Eq. (26), (29). The $C_{ef,i}$ is defined as follow

$$C_{ef,i} = \sum_{1}^{T} C_{P,i} \quad (33)$$

2) Generalized system average interruption duration index (*GSAIDI*): the average duration of the load shedding due to element failure during the simulation period. The index is defined as follows

$$\text{GSAIDI} = \left[\sum_{i=1}^{n_l} n_{l,i}(U_{ef,i} + U_{ind,i})\right] / T \sum_{i=1}^{n_l} n_{l,i} \quad (34)$$

where $U_{ind,i}$ and $U_{ef,i}$ are the load point annual power outage time due to control malfunction or power interruption within the research period T, respectively. The calculation method of $U_{ind,i}$ is shown in Eq. (27) and (30). The $U_{ef,i}$ is defined as follow

$$U_{ef,i} = \sum_{1}^{T} U_{P,i} \quad (35)$$

3) Generalized expectation of energy not supply (*GEENS*): the expected value of the power shortage due to element failure during the simulation period. The index is defined as follows

$$\text{GEENS} = \sum_{i=1}^{n_l} (E_{ef,i} + E_{cind,i}) \tag{36}$$

where $E_{ind,i}$ and $E_{ef,i}$ represent the expected value of the power shortage of the load point I due to control malfunction or power interruption within the research period T, respectively. The calculation method of $E_{ind,i}$ is shown in Eq. (28) and (31). The $E_{ef,i}$ is defined as follow

$$E_{ef,i} = \sum_{1}^{T} E_{P,i} \tag{37}$$

4) Generalized average service availability index (*GASAI*): the ratio of no blackout hours to the total power supply time requested by the users. The index is defined as

$$\text{GASAI} = \frac{\sum_{i=1}^{n_l} 8760 \cdot n_{l,i} - \sum_{i=1}^{n_l} n_{l,i}(U_{ef,i} + U_{ind,i})}{\sum_{i=1}^{n_l} 8760 \cdot n_{l,i}} \tag{38}$$

B. IMG RELIABILITY ASSESSMENT PROCESS CONSIDERING FREQUENCY CONTROL

The SMC simulation method is used to assess the system reliability [14] [26]. Considering that the failure rate of cyber element is generally low, only the first-order fault is considered in this paper. The flow chart of IMG reliability assessment based on frequency control simulation is shown in Fig. 5 and the assessment process is shown as follows

1) Initialization: Cyber and physical elements reliability parameters are collected. According to the physical network topology, the adjacency matrix is established to represent the connection relationship of cyber and physical elements [10]. Historical data for loads, wind and PV resources are given.

2) State sampling: The fault states of the cyber and physical elements are sampled by the SMC method. The running time t_{mtbf} and the repair time t_{mttr} of the element i are obtained by the Eq. (3) and (4), i.e., the running and the fault state sets of each element in the simulation period are obtained. Simulation time S_{Time} is initialized.

3) State analysis: According to the Eq. (5) - Eq.(16), the economic dispatch are solved, so that the system states during the element failure period are obtained, including the outputs of DGs and the SOC of the BESS. It should be noted that, the FMINCON function of MATLAB software is used to solve this nonlinear programming problem. Next, the faulty element type is assessed, and the quantitative assessment process shown in Fig. 3 is called to perform the calculation of the reliability indices according to the Eq. (17) – Eq.(31).

4) Assessment termination and indices statistics: If the sum of the running time $R_{\text{Time}}(i)$ and the fault time $F_{\text{Time}}(i)$ of the element i satisfies the simulation time S_{Time}, the simulation is stopped. Reliability indices of the system using Eq. (32) – Eq. (38). Otherwise repeat the steps 3) $\sim$ 4).

VI. CASE STUDY

A. TEST SYSTEM DESCRIPTION

To assess the effectiveness of the proposed methods, RBTS Bus6 F4 system [27] is adopted as one IMG system, as shown in Fig. 6. The reliability of the test system is assessed in the MATLAB software. A WTG, a PV and a DG with capacities of 3MW, 1MW and 2.5MW respectively are included in the test system. The specific parameters of the DG and BESS devices are listed in Table 2. The load frequency elastic coefficient D_{load} = 1.5 MW/Hz. 8 load points are included in the IMG, and the ratio and number of users of each load point are shown in Table 3. The load shedding strategies are formulated as follows: LP39$\sim$40, LP30, LP36$\sim$38, LP28$\sim$29. Reliability parameters are obtained from reference [10], as shown in Table 4.

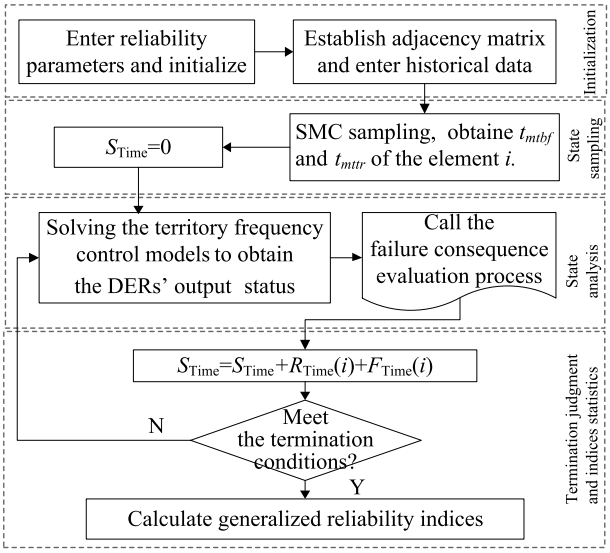

FIGURE 5. IMG reliability assessment process.

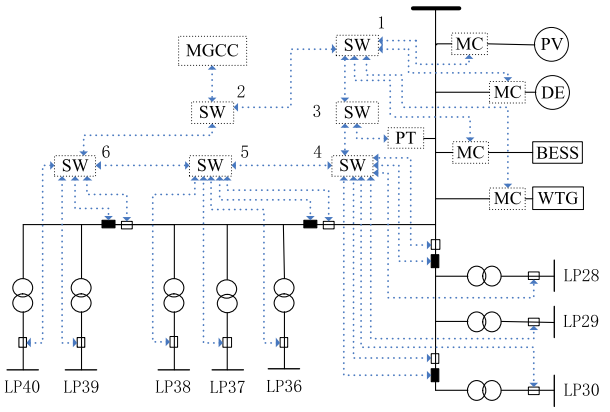

FIGURE 6. Test IMG system.

TABLE 2. Device parameters of dg and bess.

BESS		DE	
S_{nom}(MWh)	2	*Pmax D*(MW)	2.5
$P_{BESS.max}$(MW)	0.5	*A*	1
X	0.6	*d*	2584
C_{init}(million ¥)	9.6	*e*	1.7544
k_{ch}	1.05	*f*	0.0556
k_{dch}	0.95	k_{DE}	0.0946
$m_{p.BESS}$(Hz/MW)	2	$m_{p.DG}$(Hz/MW)	0.87

TABLE 3. Load ratio and number of users.

Load	Proportion	User number	Load	Proportion	User number
LP28	0.094	79	LP37	0.116	1
LP29	0.096	76	LP38	0.171	1
LP30	0.151	61	LP39	0.096	76
LP36	0.094	79	LP40	0.182	1

TABLE 4. Reliability parameters of elements.

Element	Failure rate	Repair time	Element	Failure rate	Repair time
Transformer	0.015 f/a	200h	MGCC	0.25 f/a	48h
Breaker	0.025 f/a	50h	MC	0.25 f/a	48h
Distribution line	0.018 f/a	12h	CT	0.25 f/a	48h
WTG	0.76 f/a	279h	CBC	0.25 f/a	48h
PV	0.5 f/a	40h	PT	0.25 f/a	48h
DG	1.16 f/a	100h	SW	0.2 f/a	48h
BESS	0.17 f/a	7.8h			

B. RESULTS ANALYSIS

1) IMPACTS OF CYBER ELEMENT FAILURES ON RELIABILITY

To compare the impact of different types of cyber elements failure on system reliability, the statistical results are divided into four types. **RI1**: Only the effect of random failure of physical element is considered; **RI2**: Only the effect of random failure of DI cyber element is considered; **RI3**: Only the effect of random failure of II cyber element is considered; **RI4**: the effects of random failure of all elements are considered.

The above example was simulated by Matlab software for a period of 100 years. The system rated frequency is 50Hz and the frequency is allowed to fluctuate by ±0.2 Hz. The calculation results of system reliability indices are shown in Table 5.

TABLE 5. System reliability indices.

	GASAI	GSAIFI	GSAIDI	GEENS
RI1	0.9972	0.3592	24.8814	42.8263
RI2	0.9958	0.5160	37.0734	64.2395
RI3	0.9967	0.3537	29.0104	51.0979
RI4	0.9896	1.2289	90.9652	158.1637

It can be seen from Table 5 that the reliability indices GSAIFI, GSAIDI, and GEENS in RI4 are increased by 242.12%, 265.6%, and 269.31%, respectively, compared with RI1, indicating that cyber elements failure have a significant impact on system reliability. Among them, RI3 reliability indices GSAIFI, GSAIDI, GEENS are accounted for 28.78%, 31.89% and 32.31% respectively in RI4. It can be seen that the impact of II cyber element on the reliability through the frequency control process is relatively large in the overall statistics. The load shedding caused by the failure of frequency control function cannot be ignored in the reliability assessment of IMG. At the same time, compared with the traditional reliability indices, the impact of cyber elements failure on the system load shedding through the control process can be illustrated by the proposed indices.

2) IMPACTS OF FREQUENCY FLUCTUATION RANGES ON RELIABILITY

In order to calculate and compare the changes of reliability indices under the different frequency fluctuation ranges, three examples are designed, as shown in Table 6. Other conditions are unchanged, and the statistical results of system reliability indices are shown in Table 7.

TABLE 6. Frequency fluctuation ranges.

	f_{min}(Hz)	f_{max}(Hz)
Case1(RI4)	49.8	50.2
Case2	49.5	50.5
Case3	49	51

TABLE 7. Reliability indices of different frequency ranges.

	GASAI	GSAIFI	GSAIDI	GEENS
Case1(RI4)	0.9896	1.2289	90.9652	158.1637
Case2	0.9928	1.0383	63.0345	108.5668
Case3	0.9952	0.8526	42.4332	70.7261

It can be seen from Table 7 that the index GSAIFI decreased by 15.51% and 30.62%, the index GSAIDI decreased by 30.7% and 53.35%, and the index GEENS decreased by 31.36% and 55.28%, respectively, when the frequency fluctuation range is ±0.5 Hz and ±1 Hz compared with the range of ±0.2 Hz. It is shown that the smaller the frequency fluctuation range, the worse the system reliability. The reason is that when the droop coefficients of the controllable DERs are constant, the smaller the range of frequency fluctuation, the more easily to load or power cuts due to the frequency overlimit, and system reliability is degraded in this case.

3) IMPACTS OF CYBER ELEMENT FAILURE RATES ON RELIABILITY

To investigate the impacts of cyber elements participating in frequency control on system reliability under different failure rates, the failure rates of the cyber elements MGCC, PT, and SW are increased by a factor of 20% each time to three times of the initial value. The failure rates of other elements are unchanged. The frequency fluctuation range is ±0.2Hz.

The average value of multiple calculation results is obtained and the change of the index GEENS can be used to obtain the trends in system reliability changes, as shown in Fig. 7.

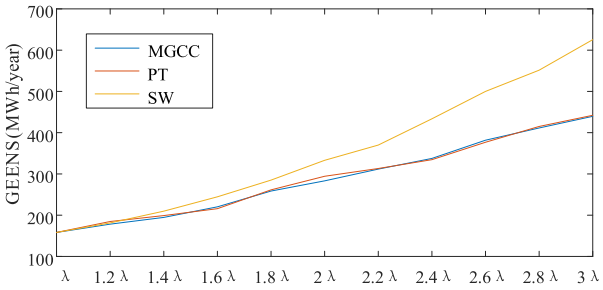

FIGURE 7. GEENS under different failure rates.

As can be seen from Fig. 7, the increase in element failure rates has a significant impact on system reliability. Among them, the change of the SW failure rate has the greatest impact on the reliability of this IMG. The effects of the MGCC and PT elements are close to each other, slightly smaller than SW. The reason is that, as shown in Fig. 6, after the failure of SWs 1, 2, and 3, the frequency control will be switched to the local mode. Due to the series relationship of multi-elements, the frequency control function failure probability caused by SW element failure is higher than that caused by element MGCC and PT, although the failure rate of SW is slightly lower than that of the MGCC and PT. Therefore, in the planning of the IMG, system reliability can be improved by improving the reliability of the SWs or by optimizing the structure of the communication network, such as using the dual-star or dual-ring communication structure including SWs standby. In addition, system reliability can be improved by adopting a way to increase the standby of MGCC and PT elements.

VII. CONCLUSION

Frequency control process and the reliability assessment of the IMG are incorporated in this paper from the perspective of CPS. The DI and II relationship between the cyber system and physical system are analyzed, and the assessment methods of IMG elements failure consequences are proposed. A set of novel reliability indices considering the malfunction of control function are introduced. SMC simulation method is used in the reliability assessment of IMGs. Simulation results show that the failure of frequency control has a great impact on the system reliability. The effect of changes in frequency fluctuation range on reliability is pointed out. Some feasible methods to improve IMG reliability have been proposed from the perspective of attenuating the effects of frequency control malfunctions. The results of this paper can lay the foundation for further in-depth study of reliability assessment that takes into account the influences of other control malfunctions, e.g., voltage regulation.

REFERENCES

[1] Z. Li, C. Zang, P. Zeng, H. Yu, and H. Li, "MAS based distributed automatic generation control for cyber-physical microgrid system," *IEEE/CAA J. Autom. Sinica*, vol. 3, no. 1, pp. 78–89, Jan. 2016.
[2] S. Karnouskos, "Cyber-physical systems in the smartgrid," in *Proc. 9th IEEE Int. Conf. Ind. Inform.*, Lisbon, Portugal, Jul. 2011, pp. 26–29.
[3] B. Falahati and Y. Fu, "A study on interdependencies of cyber-power networks in smart grid applications," in *Proc. IEEE PES Innov. Smart Grid Technol. (ISGT)*, Washington, DC, USA, Oct. 2012, pp. 1–8.
[4] A. Bidram and A. Davoudi, "Hierarchical structure of microgrids control system," *IEEE Trans. Smart Grid*, vol. 3, no. 4, pp. 1963–1976, Dec. 2012.
[5] R. Liu, C. Vellaithurai, S. S. Biswas, T. T. Gamage, and A. K. Srivastava, "Analyzing the cyber-physical impact of cyber events on the power grid," *IEEE Trans. Smart Grid*, vol. 6, no. 5, pp. 2444–2453, Sep. 2015.
[6] A. Srivastava, T. Morris, T. Ernster, C. Vellaithurai, S. Pan, and U. Adhikari, "Modeling cyber-physical vulnerability of the smart grid with incomplete information," *IEEE Trans. Smart Grid*, vol. 4, no. 1, pp. 235–244, Mar. 2013.
[7] B. Falahati, Y. Fu, and L. Wu, "Reliability assessment of smart grid considering direct cyber-power interdependencies," *IEEE Trans. Smart Grid*, vol. 3, no. 3, pp. 1515–1524, Sep. 2012.
[8] H. Hashemi-Dezaki, H. Askarian-Abyaneh, and H. Haeri-Khiavi, "Impacts of direct cyber-power interdependencies on smart grid reliability under various penetration levels of microturbine/wind/solar distributed generations," *IET Gener., Transmiss. Distrib.*, vol. 10, no. 4, pp. 928–937, Oct. 2016.
[9] W. Liu, Q. Gong, H. Han, Z. Wang, and L. Wang, "Reliability modeling and evaluation of active cyber physical distribution system," *IEEE Trans. Power Syst.*, vol. 33, no. 6, pp. 7096–7108, Nov. 2018.
[10] C. Wang, T. Zhang, F. Luo, F. Li, and Y. Liu, "Impacts of cyber system on microgrid operational reliability," *IEEE Trans. Smart Grid*, vol. 10, no. 1, pp. 105–115, Jan. 2019.
[11] Y. Han, Y. Wen, C. Guo, and H. Huang, "Incorporating cyber layer failures in composite power system reliability evaluations," *Energies*, vol. 8, no. 9, pp. 9064–9086, Aug. 2015.
[12] B. Falahati and Y. Fu, "Reliability assessment of smart grids considering indirect cyber-power interdependencies," *IEEE Trans. Smart Grid*, vol. 5, no. 4, pp. 1677–1685, Jul. 2014.
[13] T. Zhao, D. Wang, D. Lu, Y. Zeng, and Y. Liu, "A risk assessment method for cascading failure caused by electric cyber-physical system (ECPS)," in *Proc. 5th Int. Conf. Electr. Utility Deregulation Restructuring Power Technol. (DRPT)*, Nov. 2015, pp. 787–791.
[14] M. Bessani, JR. Fanucchi, and A. Delbem, "Impact of operators' performance in the reliability of cyber-physical power distribution systems," *IET Gener., Transmiss. Distrib.*, vol. 10, no. 11, pp. 2640–2646, Aug. 2016.
[15] O. Dag and B. Mirafzal, "On stability of islanded low-inertia microgrids," in *Proc. Clemson Univ. Power Syst. Conf. (PSC)*, Clemson, SC, USA, Mar. 2016, pp. 1–7.
[16] N. Rezaei and M. Kalantar, "Economic–environmental hierarchical frequency management of a droop-controlled islanded microgrid," *Energy Convers. Manage.*, vol. 88, pp. 498–515, Dec. 2014.
[17] N. Rezaei and M. Kalantar, "Smart microgrid hierarchical frequency control ancillary service provision based on virtual inertia concept: An integrated demand response and droop controlled distributed generation framework," *Energy Convers. Manage.*, vol. 92, pp. 287–301, Mar. 2015.
[18] H. Bevrani, F. Habibi, P. Babahajyani, M. Watanabe, and Y. Mitani, "Intelligent frequency control in an AC microgrid: Online PSO-based fuzzy tuning approach," *IEEE Trans. Smart Grid*, vol. 3, no. 4, pp. 1935–1944, Dec. 2012.
[19] I. Ali, S. M. S. Hussain, and S. Hussain, "Communication design for energy management automation in microgrid," *IEEE Trans. Smart Grid*, vol. 9, no. 3, pp. 2055–2064, May 2018.
[20] A. G. Tsikalakis and N. D. Hatziargyriou, "Centralized control for optimizing microgrids operation," in *Proc. Power Energy Soc. General Meeting*, Jul. 2011, pp. 1–8.
[21] D. E. Olivares, C. A. Cañizares, and M. Kazerani, "A centralized energy management system for isolated microgrids," *IEEE Trans. Smart Grid*, vol. 5, no. 4, pp. 1864–1875, Jul. 2014.
[22] C. Ahumada, R. Cárdenas, D. Sáez, and J. M. Guerrero, "Secondary control strategies for frequency restoration in islanded microgrids with consideration of communication delays," *IEEE Trans. Smart Grid*, vol. 7, no. 3, pp. 1430–1441, May 2016.

[23] S. Liu, X. Wang, and P. X. Liu, "Impact of communication delays on secondary frequency control in an islanded microgrid," *IEEE Trans. Ind. Electron.*, vol. 62, no. 4, pp. 2021–2031, Apr. 2015.
[24] G. Celli, E. Ghiani, F. Pilo, and G. G. Soma, "Reliability assessment in smart distribution networks," *Electric Power Syst. Res.*, vol. 104, pp. 164–175, Nov. 2013.
[25] R. Yokoyama, T. Niimura, and N. Saito, "Modeling and evaluation of supply reliability of microgrids including PV and wind power," in *Proc. IEEE Power Energy Soc. General Meeting-Convers. Del. Elect. Energy 21st Century*, Jul. 2008, pp. 1–5.
[26] L. X. Zhang, X. Y. Fang, and Z. H. Ni, "Reliability analysis of protection and control systems based on the effectiveness," *Power System Protection Control*, vol. 37, no. 14, pp. 63–67, Jun. 2014.
[27] R. Billinton and S. Jonnavithula, "A test system for teaching overall power system reliability assessment," *IEEE Trans. Power Syst.*, vol. 11, no. 4, pp. 1670–1676, Nov. 1996.

JING GUO received the B.S. degree in automation of electric power systems from Hebei University, Baoding, China, in 2009, and the M.S. degree in electrical engineering from North China Electric Power University, Baoding, in 2012. He is currently pursuing the Ph.D. degree in electrical information technology with North China Electric Power University, Beijing, China. His research interests include cyber-power systems and reliability assessment of power systems.

TIANYANG ZHAO (M'18) received the B.Eng., M.Eng., and Ph.D. degrees in automation of electric power systems from North China Electric Power University, Beijing, China, in 2011, 2013, and 2017, respectively. He is currently a Postdoctoral Research Fellow with the Energy Research Institute, Nanyang Technological University, Singapore. His research interests include power system operation optimization and game theory.

WENXIA LIU received the Ph.D. degree in automation of electric power systems from North China Electric Power University, Beijing, China, where she is currently a Professor with the Department of Electrical and Electronic Engineering. Her main research interest includes power system planning and operation.

JIANHUA ZHANG (M'98) received the B.S. and M.S. degrees in electrical engineering from North China Electric Power University, Baoding, China, in 1982 and 1984, respectively. He is currently a Professor with the Department of Electrical and Electronic Engineering and directs the Power Transmission and Distribution Institute, North China Electric Power University. His special fields of interests include power system security assessment, power system planning, and distributed generation. He has been the IET Fellow from the year of 2005, and also the member in the PES Committee of China National "973 Project."